Wetting on smooth micropatterned defects

Damien Debuisson, Renaud Dufour, Vincent Senez, S. Arscott

Wetting on smooth micropatterned defects

Cite as: Appl. Phys. Lett. **99**, 184101 (2011); https://doi.org/10.1063/1.3657140
Submitted: 16 June 2011 • Accepted: 06 October 2011 • Published Online: 31 October 2011

Damien Debuisson, Renaud Dufour, Vincent Senez, et al.

Wetting on smooth micropatterned defects

Damien Debuisson, Renaud Dufour, Vincent Senez, and Steve Arscott[a)]
Institut d'Electronique, de Microélectronique et de Nanotechnologie (IEMN), University of Lille, CNRS UMR-8520, Cite Scientifique, Villeneuve d'Ascq, France

(Received 16 June 2011; accepted 6 October 2011; published online 31 October 2011)

We develop a 2D model which predicts the contact angle hysteresis (CAH) introduced by smooth micropatterned defects. The defects are modeled by a smooth function, and the CAH is explained using a tangent line solution. When the liquid micro-meniscus touches both sides of the defect simultaneously, depinning of the contact line occurs and the droplet "pops-up." The defects are fabricated using the photoresist SU-8. The experimental results, using common liquids (water, isopropyl alcohol, and ethylene glycol), agree well with the predictions of the model. The profile of the defect has a large influence on the CAH. © *2011 American Institute of Physics*.
[doi:10.1063/1.3657140]

When a sessile droplet contracts (e.g., via evaporation) or swells (e.g., via condensation), the contact line (i.e., the liquid-vapor-solid interface) moves according to the contact angle hysteresis (CAH);[1–7] this effect is fundamental for many modern applications.[8–11] In contrast to tuning the CAH by controlling defect length,[12] here, we demonstrate that the CAH can be modified using the defect profile corresponding to a tangent line solution for the depinning of the micro-meniscus of a droplet.

We consider here the CAH introduced by a smooth defect[5] in an idealized flat surface. We assume that the defect can be modeled by a function $h(x)$ which is smooth in the mathematical sense. First, let us consider the *microscopic* contact angle $\bar{\theta}$ in the vicinity of the micro-meniscus. If the contact line moves (Fig. 1), we consider $\bar{\theta}$ is constant relative to the surface tangent. We assume the profile of the micro-meniscus to be that of a straight line. Fig. 1(a) is an advancing contact line where the micro-meniscus does not touch the right hand side (rhs) of the defect as the contact line moves over the defect. Fig. 1(b) is an advancing contact line where the micro-meniscus does touch the rhs of the defect. Fig. 1(c) is a receding contact line where the micro-meniscus does not touch the left hand side (lhs) of the defect. Fig. 1(d) is a receding contact line where the micro-meniscus *does touch* the lhs of the defect. In all cases, the centre of the droplet is considered to be to the left of the defect. $\bar{\theta}^*_{r,a}$ in Fig. 1 refers to the effective microscopic contact angle with respect to the horizontal plane when the contact line depins from the defect.

Let us now consider the case of the receding contact line in more detail (the arguments apply equally to the advancing contact line via symmetry). When the contact line encounters the defect, it moves down the rhs ($x > 0$) of the defect, $\bar{\theta}_r$ remains constant; the result of this is that the macroscopic contact angle with respect to the horizontal plane reduces. It is important now to make a physical distinction between the liquid micro-meniscus touching the lhs ($x < 0$) of the defect or not.

If the micro-meniscus does not touch the opposite side of the defect [Fig. 1(c)] then the *effective* receding contact angle introduced by the defect is given by $\bar{\theta}^*_r = \bar{\theta}_r - \tan^{-1}[h'(x_p)]$, where x_p is the point of inflection[1] on the rhs of $h(x)$.

If the liquid meniscus touches the lhs of the defect[3] (at $x = x_t$), then $\bar{\theta}^*_r$, which is given by $\tan^{-1}[h'(x_t)]$, is equal to $\bar{\theta}_r - \tan^{-1}[h'(x_i)]$; in this case, the relationship between $\bar{\theta}_r$ and $\bar{\theta}^*_r$ is non-linear. This is the tangent line at x_t which also intersects $h(x)$ at $x = x_i$; this case is illustrated in Fig. 1(d). By symmetry, $\bar{\theta}^*_a$ is given by $\bar{\theta}_a - \tan^{-1}[h'(x_i)]$ by using the same arguments above but with the contact line moving from left to right [Fig. 1(b)]. Continuing the receding angle case, once the micro-meniscus touches the lhs of the defect at x_t, it will break as the contact line will not be stable at x_t; as a consequence, the contact line will depin. Thus, the required tangent line cuts $h(x)$ at two points: the tangent point (x_t) on the lhs of the defect and the intersection point (x_i) on the rhs of the defect. Hence, we can write $\bar{\theta}^*_{r,a} = \tan^{-1}[h'(x_t)]$ and $\tan^{-1}[h'(x_t)] = \bar{\theta}_{r,a} - \tan^{-1}[h'(x_i)]$ together with the tangent line $h(x_t) - h(x_i) = h'(x_t)(x_t - x_i)$. As $h(x)$ is a smooth function, it follows that we should be able to resolve the problem in terms of simple parameters (the defect depth h_0, the defect width w and $\bar{\theta}_{r,a}$).

The micropatterned defects can be modeled using a cosine function over a single period: $h(x) = -\frac{1}{2}h_0(\cos(2\pi x/w) + 1)$, where h_0 and w are described above. Two tangent line solutions exist for the given values of $\bar{\theta}_r$ and $\bar{\theta}_a$; the required solution is the tangent line which intersects $h(x)$ above its

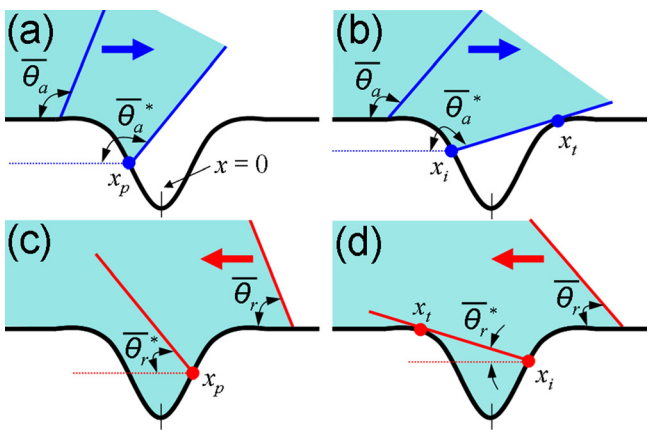

FIG. 1. (Color online) A contact line moving across a surface containing a smooth defect for (a) and (b) an advancing contact line and (c) and (d) a receding contact line.

[a)]Electronic mail: steve.arscott@iemn.univ-lille1.fr.

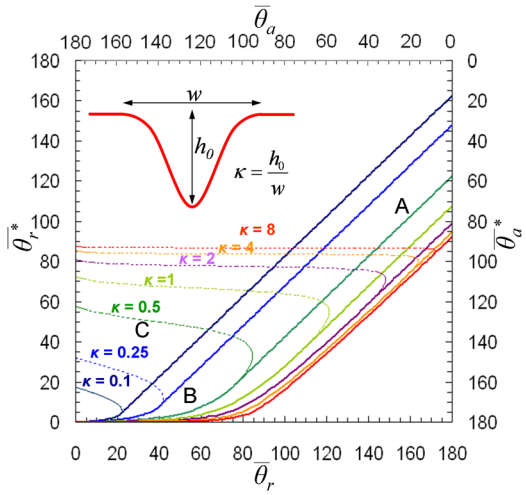

FIG. 2. (Color online) Theoretical curves for of $\overline{\theta}_{r,a}^*$ as a function of $\overline{\theta}_{r,a}$ on defects of differing aspect ratio κ. The linear part (A) of the curve corresponds to the case where the micro-meniscus does not touch the opposite side of the defect when moving across it. The non-linear part of the curve (B) corresponds to the first tangent line solution. The dashed non-linear part of the curve (C) corresponds to the second tangent line solution. Inset shows the dimensions of the defect.

point of inflection as this is where the micro-meniscus initially touches both sides of the defect simultaneously. A numerical solution to the equations above leads to the curves given in Fig. 2 which shows the calculated values of $\overline{\theta}_{r,a}^*$ as a function of $\overline{\theta}_{r,a}$.

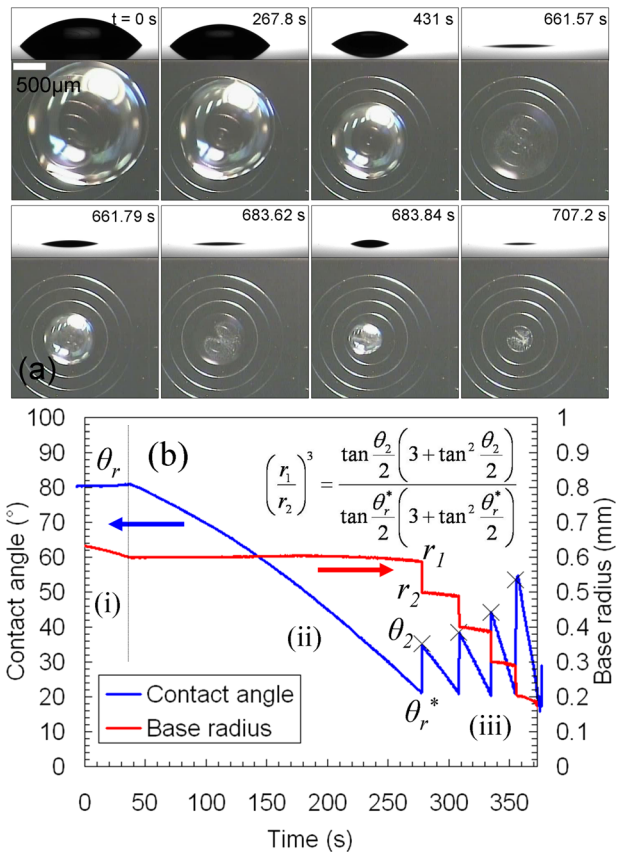

FIG. 3. (Color online) (a) Plan and side view optical images of a droplet (H_2O) evaporating on a micropatterned surface (SU-8) composed of concentric circle defects separated by 200 μm. (b) Variation of contact angle and droplet base radius for a droplet (IPA/H_2O) on smooth defects separated by 100 μm defined in SU-8 covered with FC. (× indicates values of θ_2 calculated using the inset equation).

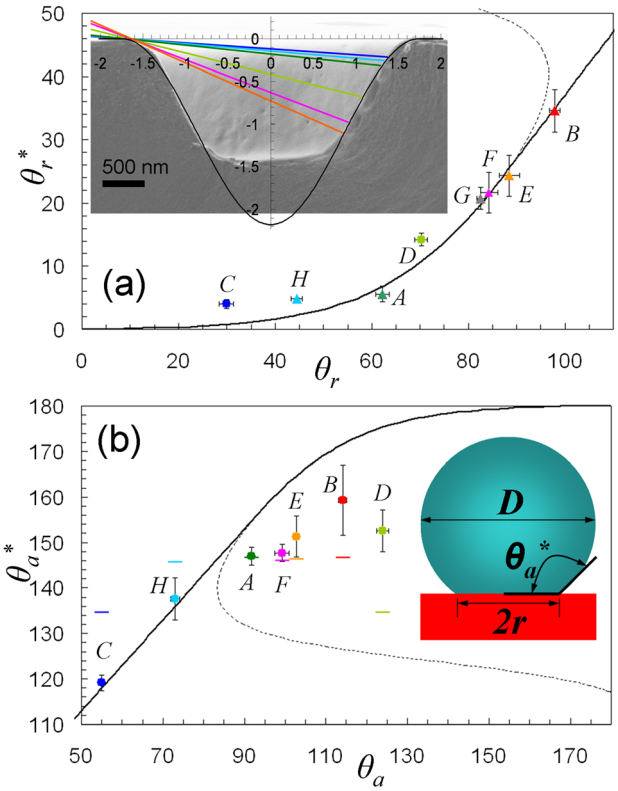

FIG. 4. (Color online) Experimental values of the effective receding and advancing contact angles on a defect for various liquids. (a) The effective receding contact angle (θ_r^*). H_2O on SU-8 (A), H_2O on FC (B), $C_2H_6O_2$ on SU-8 (C), $C_2H_6O_2$ on FC (D), IPA/H_2O (2.5/97.5) on FC (E), IPA/H_2O (5/95) on FC (F), IPA/H_2O (10/90) on FC (G), and IPA/H_2O (10/90) on SU-8 (H). The predicted curve (black) using the model is also shown (using an aspect ratio $\kappa = 0.625$). Inset shows an SEM image of a cross-section of a defect formed using photolithography of SU-8; the 100 nm thick fluorocarbon layer deposited onto the SU-8 surface is visible. The lines represent the tangent line solutions for the various liquids. (b) The effective advancing contact angle (θ_a^*) on a defect. The predicted curve (black) using the model is also shown (using an aspect ratio $\kappa = 0.625$). The bars represent the calculated contact angle when the droplet diameter is equal to the capillary length of the liquid. Inset show a droplet resting on a solid surface, $D = 2r/\sin(\pi - \theta_a^*)$. (Triangles: evaporation data; circles: syringe data).

Due to symmetry, the tangent line solution applies to both receding and advancing contact lines as $\overline{\theta}_a^* = \pi - \overline{\theta}_r^*$ (this only holds for a defect which is symmetrical around $x = 0$). Note that Fig. 2 indicates that there can be two values of $\overline{\theta}_{r,a}^*$ for a given $\overline{\theta}_{r,a}$; the dashed lines correspond to the second tangent line solution and do not physically occur here as the micro-meniscus touches the other side of the defect and depins at the first tangent line solution. It should also be noted that the solutions are scale-independent, i.e., a tangent line solution is true for *any* cosine function (defect) having a ratio $\kappa = h_0/w$, as shown in the inset of Fig. 2. This assumption holds since the micro-meniscus is considered to be a straight line with respect to the defect size.

In order to test our model, we fabricated[13] micropatterned surfaces using the photoresist SU-8. A photolithographic mask enabled the formation concentric circles (trench-like defects) of diminishing diameters (0.1–2 mm) (Fig. 3). The surfaces were also covered with a thin coating (~100 nm) of fluorocarbon (FC).[13]

The contact angle measurements were performed in a class ISO 5/7 cleanroom ($T_A = 20\,°C \pm 0.5\,°C$; $RH = 45\% \pm 2\%$) using a contact angle meter (Kruss, Germany).

TABLE I. Summary of findings. (a) SU-8 and (b) FC.

	Experiment.				Calculations	
Liquid	θ_r	θ_a	θ_r^*	θ_a^*	$\bar{\theta}_r^*$	$\bar{\theta}_a^*$
H_2O[(a)]	62.2° ± 2.8	91.8° ± 0.5	5.6° ± 1.3	147° ± 2	6.8°	154.7°
H_2O[(b)]	97.9° ± 2.3	114.1° ± 2.1	34.6° ± 3.4	159.3° ± 7.7	35°	171.6°
$C_2H_6O_2$[(a)]	29.9° ± 1.5	55° ± 0.6	4° ± 0.7	119.2° ± 1.7	0.8°	118°
$C_2H_6O_2$[(b)]	70.2° ± 1.3	123.9° ± 1.5	14.2° ± 1	152.6° ± 4.7	10.7°	175.3°
IPA/H_2O (2.5/97.5)[(b)]	88.5° ± 4.3	102.7° ± 1.4	24.3° ± 3.3	151.3° ± 4.5	25.5°	164.5°
IPA/H_2O (5/95)[(b)]	84.3° ± 1.8	98.3° ± 1	21.6° ± 3.2	147.7° ± 1.8	21.3°	161°
IPA/H_2O (10/90) [(a)]	44.5° ± 1.2	72.9° ± 1.1	4.9° ± 0.1	137.6° ± 4.6	2.3°	135.9°

Observation of menisci at the millimeter-scale is relatively simple,[14] whereas micro-menisci contact angles measurements are challenging.[15–17] Here, the CAH was measured using droplet expansion (syringe pump) and evaporation.[18] We verified that evaporation and syringe methods give the same results for contact angle measurements. In order to measure the macroscopic receding and advancing contact angles (θ_r, θ_a, θ_r^*, θ_a^*) using the syringe method, a small droplet of liquid ($vol \sim 0.3$ nL) was positioned onto the smallest concentric circle ($\varphi = 100\,\mu$m) at the centre of the micropatterned surface and swelled using a syringe pump (1–5 μL min^{-1}) in order to measure θ_a and θ_a^*. Once the droplet diameter was larger than the largest concentric circle in the micropattern ($\varphi = 2$ mm), the droplet volume was reduced using the syringe (1–5 μL min^{-1}) in order to measure θ_r and θ_r^*. For the evaporation tests, a droplet ($vol \sim 2\,\mu$L) was placed on the micropatterned surface and allowed to slowly evaporate (unforced), whilst the values of θ_r and θ_r^* were recorded as a function of time. This evaporation method was not possible for ethylene glycol due to a low vapor pressure at room temperature;[19] however, evaporation tests were possible using IPA/H_2O solutions as the vapor pressure of IPA and of water are very similar at room temperature.[19]

Fig. 3(a) shows a typical droplet evaporation sequence recorded for a micropattern. The contact line becomes pinned onto a circular defect at $t = 431$ s. The apparent contact angle reduces until the effective contact angle θ_r^* is attained, whereby the droplet suddenly depins and "pops-up" at $t = 661$ s; the droplet subsequently pins to the next smallest circle defect and the process repeats one more time. Fig. 3(b) shows the data gathered over a period of 375 s for an evaporating droplet (IPA/H_2O) on a FC coated SU-8 surface. Three distinct phases are apparent: Phases (1) and (2) correspond to droplet evaporation at constant contact angle with diminishing droplet base radius[18] followed by constant base radius and diminishing contact angle.[18] When the droplet is not pinned to a defect and phase (3), an evaporating droplet depinning from circle to circle where the contact angle follows a saw-tooth variation[3,4,6] with θ_r^* constant. This sawtooth profile increases in amplitude according to the equation given in the inset. As the droplet depins from circle to circle, since the volume is constant at each depinning, θ_2 must be larger at each depinning cycle (distance between circles D constant); the evaporation between the depinnings is described as in Ref. 18.

Fig. 4 shows a plot of the experimentally obtained values of θ_r^* and θ_a^* as a function of θ_r and θ_a for various liquids on surfaces containing smooth micropatterned defects. Our measurements indicate that the microscopic model can accurately predict the values of θ_r^* introduced by the defect, thus giving a strong evidence for the tangent line solution model for the macroscopic CAH introduced by a smooth defect. The inset to Fig. 4(a) illustrates good agreement between the experimental defect and the model. Despite the defect not being a perfect cosine shape, the parameters h_0 and w enable a good fit between the real defect shape and the model in the region where the liquids depin. Theoretical[3] and experimental[4] studies on CAH induced by sinusoidal defects have been performed, although neither resolved the tangent line depinning problem.

Let us now consider the experimental results for θ_a^* shown in Fig. 4(b). Due to the finite needle diameter, the values of θ_a^* were measured at droplet base radii between 0.5–1 mm. Two liquid/surface combinations fit very well with the predictions of the model and five deviate from the model. In order to explain this, horizontal bars have been added to Fig. 4(b), which indicate the value of contact angle calculated using a base radius r of 0.75 mm and equating the droplet diameter D to the capillary length $(\gamma/\rho g)^{1/2}$ of the liquid. These bars represent the maximum values of θ_a^* before gravity becomes non-negligible[3,4] and vibrations are known to cause depinning.[20] Table I gives a summary of all results.

[1] R. Shuttleworth and G. L. J. Bailey, Discuss. Faraday Soc. **3**, 16 (1948).
[2] R. E. Johnson and R. H. Dettre, J. Phys. Chem. **68**, 1744 (1964).
[3] C. Huh and S. G. Mason, J. Colloid Interface Sci. **60**, 11 (1977).
[4] J. P. Oliver, C. Huh, and S. G. Mason, Colloids Surf. **1**, 79 (1980).
[5] J. F. Joanny and P. G. De Gennes, J. Chem. Phys. **81**, 552 (1984).
[6] H. Kusumaatmaja and J. M. Yeomans, Langmuir **23**, 6019 (2007).
[7] M. Reyssat and D. Quéré, J. Phys. Chem. B **113**, 3906 (2009).
[8] R. Blossey, Nature Mater. **2**, 301 (2003).
[9] X. J. Feng and L. Jiang, Adv. Mater. **18**, 3063 (2006).
[10] G. M. Whitesides and B. Grzybowski, Science **295**, 2418 (2002).
[11] J. B. Hannon, S. Kodambaka, F. M. Ross, and R. M. Tromp, Nature **440**, 69 (2006).
[12] D. Debuisson, V. Senez, and S. Arscott, Appl. Phys. Lett. **98**, 184101 (2011).
[13] D. Debuisson, V. Senez, and S. Arscott, J. Micromech. Microeng. **21**, 065011 (2011).
[14] W. Choi, A. Tuteja, J. M. Mabry, R. E. Cohen, and G. H. McKinley, J. Colloid Interface Sci. **339**, 208 (2009).
[15] H. Rathgen, K. Sugiyama, C.-D. Ohl, D. Lohse, and F. Mugele, Phys. Rev. Lett. **99**, 214501 (2007).
[16] C. Journet, S. Moulinet, C. Ybert, S. T. Purcell, and L. Bocquet, Europhys. Lett. **71**, 104 (2005).
[17] J.-G. Fan and Y.-P. Zhao, Nanotechnology **19**, 155707 (2008).
[18] R. G. Picknett and R. Bexon, J. Colloid Interface Sci. **61**, 336 (1977).
[19] *CRC Handbook of Chemistry and Physics*, 69th ed., edited by R. C. Weast (CRC, Florida, USA).
[20] P. Brunet, J. Eggers, and R. D. Deegan, Eur. Phys. J. **166**, 11 (2009).